Photonic band gap of two-dimensional triangular photonic crystals with broken structural and rotational symmetries

K. P. Chang and S. L. Yang

Citation: Journal of Applied Physics **100**, 073104 (2006); doi: 10.1063/1.2356992
View online: http://dx.doi.org/10.1063/1.2356992
View Table of Contents: http://scitation.aip.org/content/aip/journal/jap/100/7?ver=pdfcov
Published by the AIP Publishing

Photonic band gap of two-dimensional triangular photonic crystals with broken structural and rotational symmetries

K. P. Chang and S. L. Yang[a)]
Department of Electrophysics, National Chiao Tung University, Hsinchu 30050, Taiwan, Republic of China

(Received 14 March 2006; accepted 3 August 2006; published online 9 October 2006)

Three deformed and two rotational structures are constructed to study the effect of structural and rotational symmetries on the gap widths of *E*- and *H*-polarization bands in photonic crystals. The band structures and field patterns of a triangular lattice of hollow tellurium (Te) rods are calculated using the plane-wave method. The *H*-polarization band gaps are strongly affected by the interaction between the fields of the rods as the rods are deformed and affected by the reduction in the rotational symmetry as whole rods are rotated. Only the shapes of the rods affect the *E*-polarization band gaps as the rods are either deformed or rotated. Moreover, *H*-polarization modes determine the absolute photonic band gap (PBG) width as the rods are rotated, whereas *E*-polarization modes determine the absolute PBG width as the rods are deformed. © *2006 American Institute of Physics*.
[DOI: 10.1063/1.2356992]

I. INTRODUCTION

The physical characteristics of photonic crystals (PCs) and their use in devices have attracted much attention in recent years owing to their various interesting properties and several innovative applications.[1–5] Photonic crystals with properly designed dielectric constants, structural symmetry, and filling ratio may have polarization-independent photonic band gaps (PBGs), i.e., the so-called absolute PBG.[6–9] Absolute PBG materials can be used for confining or controlling the propagation of waves.

Some works have demonstrated that the absolute PBGs of two-dimensional (2D) photonic crystals can be widened by reducing the symmetry of the rods; such crystals are typically designed with triangular, square, and hexagonal lattices of air or dielectric rods with various shapes and cross sections.[10–14] A hollow oval rod embedded in a triangular lattice can exhibit a large PBG at high normalized frequencies.[15] However, the effect of structural and rotational symmetries associated with the deformation and rotation of rods on *E*-polarization (with the electric field parallel to the rods) and *H*-polarization (with the magnetic field parallel to the rods) band gaps of the system has not been studied thoroughly.

This work investigates the effect of structural and rotational symmetries on the *E*-polarization and *H*-polarization band gaps of hollow rods embedded in a triangular lattice. The plane-wave method is employed to calculate the band structures and field patterns. The symmetry of hollow rods is more complex than that of solid rods because the former can be broken by deforming and rotating inner and shell rods. Three deformed structures, involving inner rod deformation, shell-rod deformation, and whole rod deformation, are considered to explore the effect of structural deformation on the band structures. Two rotational structures—inner rod rotation and whole rod rotation—are introduced to investigate the effect of rotational symmetry on the band structures. The correlations between the hollow structures and PBGs can be reasonably explained, and the scattering mechanisms are systematically examined.

II. THEORY

Figure 1 displays the geometry of the 2D triangular lattice of hollow oval rods, where a is the lattice constant, $\mathbf{a}_1 = a(1,0)$, and $\mathbf{a}_2 = a(1/2, \sqrt{3}/2)$ are the basic vectors of the triangular lattice. Each hollow rod comprises an inner rod (hollow portion) with isotropic dielectric constant ε_r, and an outer shell with anisotropic dielectric constants ε_e and ε_o. The structured background is homogeneous with dielectric constant ε_b. The dimensions of the inner rod and the outer shell are, in units of lattice constant a and in the directions of the major and minor axes, (ℓ_1, w_1) and (ℓ_2, w_2), respectively. The terms $\alpha_1 = \ell_1/w_1$ and $\alpha_2 = \ell_2/w_2$ are used for convenience.

The electromagnetic fields in the 2D photonic crystals are given by Maxwell's equation,

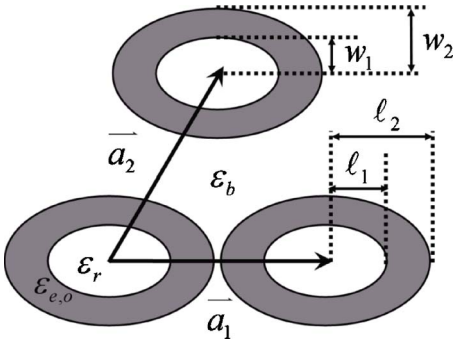

FIG. 1. Schematic configuration of a triangular lattice with hollow oval Te rods.

[a)]Electronic mail: slyang@mail.nctu.edu.tw

$$\nabla \times \left[\frac{1}{\varepsilon(\mathbf{r})} \nabla \times \mathbf{H}(\mathbf{r}) \right] = \frac{\omega^2}{c^2} \mathbf{H}(\mathbf{r}), \tag{1}$$

where $\mathbf{H}(r)$ is the magnetic field, $\varepsilon(\mathbf{r})$ is a position-dependent dielectric constant, ω is the angular frequency, and c is the speed of light in a vacuum. For periodic systems, the magnetic field $\mathbf{H}(\mathbf{r})$ and the dielectric function $\varepsilon(\mathbf{r})$ can be expressed as sums of plane waves,

$$\mathbf{H}(\mathbf{r}) = \sum_{\mathbf{G}} \sum_{\lambda=1,2} h_{G,\lambda} \hat{e}_\lambda e^{i(\mathbf{k}+\mathbf{G})\cdot\mathbf{r}} \tag{2}$$

and

$$\varepsilon(\mathbf{r}) = \sum_{\mathbf{G}} \varepsilon(\mathbf{G}) e^{i\mathbf{G}\cdot\mathbf{r}}, \tag{3}$$

where $h_{G,\lambda}$ is a coefficient of the $\mathbf{H}$ component, $\mathbf{k}$ is the wave vector in the Brillouin zone, and $\mathbf{G}$ is the reciprocal-lattice vector, respectively. Two independent polarizations characterized by the unit vectors $\hat{e}_\lambda(\lambda=1,2)$ are perpendicular to the propagation vector $(\mathbf{k}+\mathbf{G})$. Under Fourier transform, the coefficient of $\varepsilon(\mathbf{G})$ is defined as

$$\varepsilon(\mathbf{G}) = \frac{1}{A_{\text{cell}}} \int_{\text{cell}} \varepsilon(\mathbf{r}) e^{-i\mathbf{G}\cdot\mathbf{r}} dr, \tag{4}$$

where A_{cell} is the area of the primitive cell of the lattice. So Eq. (1) can be expressed in a matrix form,

$$\sum_{G'} |\mathbf{k}+\mathbf{G}||\mathbf{k}+\mathbf{G}'| \begin{bmatrix} \hat{e}_2 \cdot \varepsilon^{-1}_{G,G'} \cdot \hat{e}'_2 & -\hat{e}_2 \cdot \varepsilon^{-1}_{G,G'} \cdot \hat{e}'_1 \\ -\hat{e}_1 \cdot \varepsilon^{-1}_{G,G'} \cdot \hat{e}'_2 & \hat{e}_1 \cdot \varepsilon^{-1}_{G,G'} \cdot \hat{e}'_1 \end{bmatrix} \times \begin{bmatrix} h_{1,G'} \\ h_{2,G'} \end{bmatrix} = \frac{\omega^2}{c^2} \begin{bmatrix} h_{1,G} \\ h_{2,G} \end{bmatrix}, \tag{5}$$

where $\varepsilon^{-1}_{G,G'} = \varepsilon^{-1}(\mathbf{G}-\mathbf{G}')$ represents the inverse of the matrix $\varepsilon(\mathbf{G}-\mathbf{G}')$. The eigenvalue equation (5) can then be solved using matrix diagonalization technique.

The dielectric constant of hollow structure can be expressed as

$$\varepsilon(\mathbf{r}) = \varepsilon_b + (\varepsilon_{e,o} - \varepsilon_b) S_{\text{shell}}(\mathbf{r}) + (\varepsilon_r - \varepsilon_b) S_{\text{rod}}(\mathbf{r}), \tag{6}$$

where $S_{\text{shell}}(\mathbf{r})$ and $S_{\text{rod}}(\mathbf{r})$ are the functions of the outer shell and the inner rod, respectively. The magnitudes of these two functions are set to unity inside the interesting region and zero outside. The Fourier transform of $\varepsilon(\mathbf{r})$ is

$$\varepsilon(\mathbf{G}) = \varepsilon_b \delta_{G,0} + (\varepsilon_{e,o} - \varepsilon_b) \frac{2f_{\text{shell}}}{\sqrt{g_2(\theta_2)}\ell_2} J_1(\sqrt{g_2(\theta_2)}\ell_2) + (\varepsilon_r - \varepsilon_b) \frac{2f_{\text{rod}}}{\sqrt{g_1(\theta_1)}\ell_1} J_1(\sqrt{g_1(\theta_1)}\ell_1). \tag{7}$$

The second and third terms represent $\varepsilon(\mathbf{G})$ for the shell and the inner rods, respectively. The factors $f_{\text{shell}}=(\pi\ell_2 w_2)/A_{\text{cell}}$ and $f_{\text{rod}}=(\pi\ell_1 w_1)/A_{\text{cell}}$ are the ratios of the area of the outer shell and of the inner rod to the area of a primitive unit cell. J_1 is the Bessel function of the first kind. The function $g_1(\theta_1)$ represents the magnitude of the reciprocal-lattice vector as inner rods are rotated through an angle θ_1, and the function $g_2(\theta_2)$ represents the magnitude of the reciprocal-lattice vector as the outer shells are rotated through an angle θ_2. They are given by

$$g_{1,2}(\theta) = G_x^2(\cos^2\theta_{1,2} + \alpha_{1,2}^{-2}\sin^2\theta_{1,2}) + G_y^2(\sin^2\theta_{1,2} + \alpha_{1,2}^{-2}\cos^2\theta_{1,2}) + 2G_xG_y \sin\theta_{1,2}\cos\theta_{1,2}(1-\alpha_{1,2}^{-2}), \tag{8}$$

where G_x and G_y are the x- and y-axial components of $\mathbf{G}$, respectively. The band structures for such anisotropic photonic crystals can be calculated in the same way as for isotropic crystals. In this study, 1000 plane waves were adopted, and the computational errors in the E- and H-polarization modes for each case were estimated to be less than 1%.

III. RESULTS AND DISCUSSION

This study calculates photonic-band structures of hollow tellurium (Te) rods in a triangular lattice. The hollow rods with cross section in the size of micrometers could be patterned with the nanolithographic technology. However, Te is not the popular material for the current lithographic technology; it is still not well developed for making Te microstructures to photonic crystals. The usage of Te in this study is taking advantage of its high refractive index. The high index of refractivity allows us to tune the absolute PBG within a large extent. Furthermore, the large difference between the extraordinary and the ordinary refractive indices also permits us to study more flexibly the effects of the structural and rotational symmetries on the PBG of hollow structure. Te has anisotropic optical properties with approximate extraordinary refractive index $n_e=6.2$ and ordinary refractive index $n_o=4.8$ in the wavelength regime between 3.5 and 14 μm.[15–17] The absorption coefficient of Te in the infrared region is less than 1 cm^{-1}.[18] In the appropriate infrared range and for a photonic crystal with limited size, the refractive indices of Te can be treated as constants and the absorption effect can be neglected in the calculation.[15,16] In fact, a preliminary calculation shows that very small uncertainty involved in our calculation when the refractive indices of Te is assumed as constants and the absorption effect is neglected. The axis of Te rod is set to be parallel to the extraordinary axis and provides different refractive indices for the E- and H-polarization modes in the structure. The band gaps of two modes are overlapped to give the absolute PBG width of the photonic crystal system.

The dielectric constants of the background material and the inner holes are set to $\varepsilon_b=\varepsilon_r=1$. Three deformed structures, A, B, and C, are considered to investigate the effect of the shape of a hollow rod on the PBG. The structures are deformed by altering the factors α_1 and α_2, which are designed to prevent overlap between nearest neighboring rods. The optimal parameters of major axes of inner rods and outer shells, taking as $\ell_1=0.27a$ and $\ell_2=0.48a$, are adopted throughout the simulation to study how the structural and rotational symmetries affect the PBG of hollow structure. Basically, the choice of $\ell_1=0.27a$ and $\ell_2=0.48a$ provides us eclectically the largest two absolute PBG widths. And both absolute PBG widths decrease with increasing ℓ_2 for a constant ℓ_1 but fluctuate with varying ℓ_1 for a constant ℓ_2.

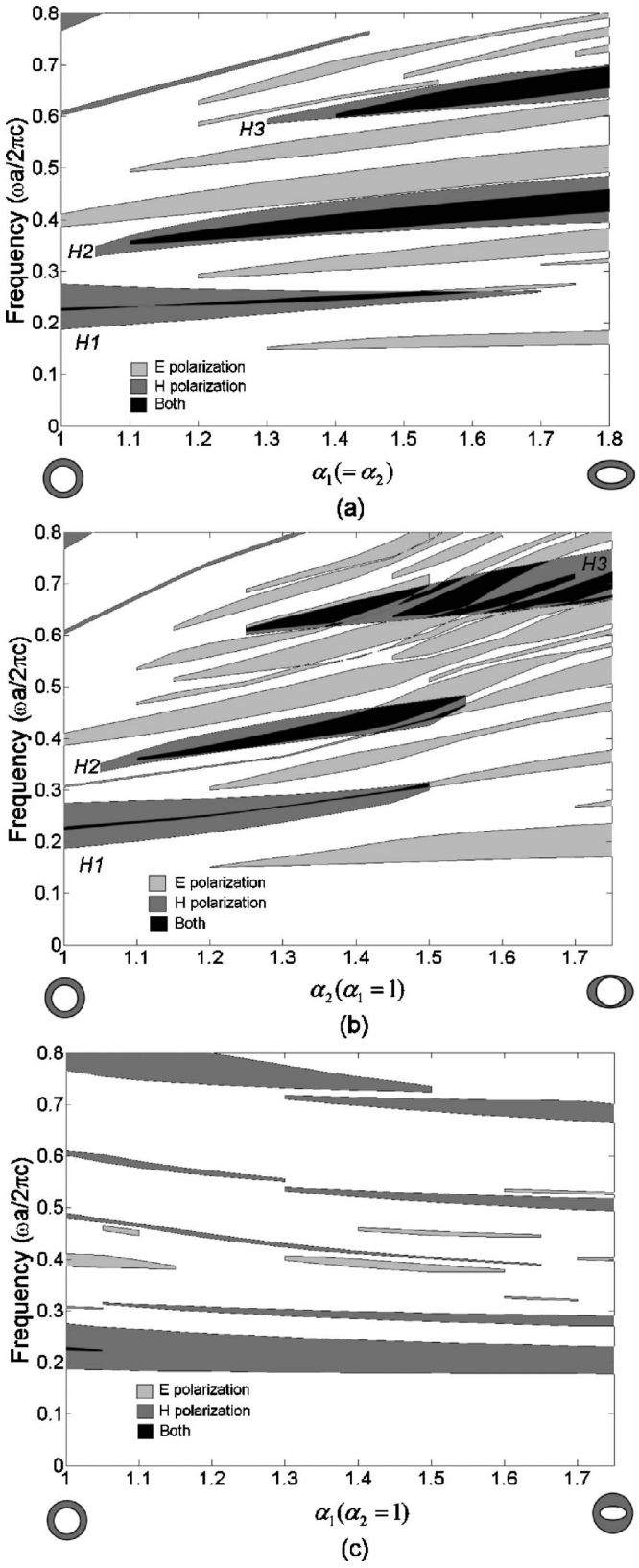

FIG. 2. Gap maps of (a) structure *A*, $\alpha_1=\alpha_2$, (b) structure *B*, $\alpha_1=1$; and (c) structure *C*, $\alpha_2=1$. The major-axis lengths of shell and inner rods are fixed to $\ell_1=0.27a$ and $\ell_2=0.48a$.

Structures *A* are designed such that the lengths of the minor axes of the inner and shell rods are simultaneously reduced to equalize α_1 and α_2. Figure 2(a) presents the dependence of the gap map on α_1. Many gaps appear for *E*-polarization modes, and three gaps appear for *H*-polarization modes between 0.2 and $0.8(\omega a/2\pi c)$. The width of the H1 gap is maximal at $\alpha_1=1$, and is zero at approximately $\alpha_1=1.7$. H2 and H3 gaps do not appear in the hollow circular structure, until structural symmetry is broken. As shown in the diagram, this configuration generally has three absolute PBGs and the *E*-polarization modes dominate the absolute PBG widths.

Structures *B* with circular inner rods ($\alpha_1=1$) and vertically deformed shell rods are considered. That is, the structural symmetry of the inner rod is retained, whereas that of the shell rod is broken. Figure 2(b) presents the calculations. When α_2 exceeds 1.35, the gap widths of the *E*-polarization modes vary more than those in structures *A*, drastically reducing the absolute gap widths. However, the width of the *H*-polarization gap as a function of α_2 is quite similar to those in structures *A*. The width of the H1 gap declines while that of the H3 gap increases as α_2 increases. The behavior of the H3 gap width can be elucidated by wave scattering in the hollow rods. The propagation of light of short wavelength in the hollow rods depends strongly on the shape of rod, so resonance can be easily produced. Therefore, the shape of the rod determines the high-frequency gaps of *H*-polarization modes. With respect to the H1 gap, light with long wavelength cannot easily be trapped with resonance in the rods, so the interaction among the fields of the rods must be examined in detail. In the *H*-polarization modes, fields are oriented in the *x*-*y* plane and the tangential fields that connect nearest-neighboring rods must be forced to penetrate regions of air to satisfy the continuity boundary condition.[19] Accordingly, the variation in the *y*-directional length influences the fraction of energy in the dielectric regions, and thereby alters the low-frequency gap width.

Structures *C* have circular shell rods ($\alpha_2=1$) and deformed inner rods. The air-space sizes between the rods are very thin in such structures. As shown in Fig. 2(c), the width of the H1 gap is almost independent of α_1, because the air-space sizes among the rods are kept invariable, while the width of the H3 gap varies drastically, since the rods are deformed. Furthermore, the width of the *E*-polarization gap may not be increased by reducing the structural symmetry of the inner rods, so no absolute PBG is present in such structures.

The calculated band gaps of structures *A*, *B*, and *C* show that the *E*-polarization modes dominate the absolute PBG widths. The field patterns of each structure are examined to investigate the effect of structural symmetry on the *E*-polarization modes. Figures 3(a)–3(d) show the level distribution of the displacement field in hollow circular structures and deformed structures *A*, *B*, and *C*, respectively. Each figure plots the distribution of magnitudes of the displacement field associated with the seventh band at the *K*-symmetry point. The fields in structure *A* are concentrated in the dielectric regions for all $\alpha_1(=\alpha_2)$ values. However, the deformation in the shell rods of structure *B* strongly influences the field distribution. In particular, the displacement fields in the thin section are expelled from the dielectric region and are distributed nonuniformly within the rods, so the gap widths in the *E*-polarization modes of structure *B* vary

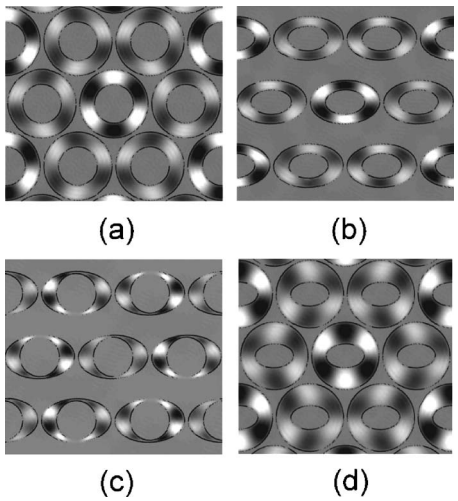

FIG. 3. Displacement-field distribution of *E*-polarization modes inside the hollow rods in the (a) hollow circular structure, $\alpha_1=\alpha_2=1$, (b) structure *A* with $\alpha_1=\alpha_2=1.6$, (c) structure *B* with $\alpha_1=1$, $\alpha_2=1.6$; and (d) structure *C* with $\alpha_1=1.6$, $\alpha_2=1$ at *K*-symmetry point.

more than those of structure *A*. Figure 3(d) shows the field patterns in structure *C*. The variation in the field distribution is not as strong as that in structure *B* as the geometry of the rods is changed. This result may be attributed to the fact that the sizes of the inner rods are not large enough and the field distribution is similar to that in the hollow circular structure.

The symmetry of the hollow structure can also be broken by rotating the inner and shell parts without changing the geometric parameters. Two rotations, inner and whole rod rotations, under the geometric parameter constant $\alpha_1=\alpha_2$, are considered herein. All structures have the same filling fraction but are differently orientated with respect to the triangular lattice. The inner rod rotation is rotated with a period of 90°, while the whole rod rotation is rotated with a period of 60°. The dependence of the *H*-polarization gap widths on rotating angle is examined. Figures 4(a) and 4(b) show the H1 gap widths associated with inner and whole rod rotations for various α_1. The width of the H1 gap slightly decreases under the inner rod rotation as the angle of rotation increases. Notably, the air-space sizes among the rods remain constant under the inner rod rotation through an arbitrary angle, indicating that the interaction between the fields of the rods affects the *H*-polarization modes almost equally at any angle of rotation. At whole rod rotation drastically increases the width of the H1 gap; the gap width is largest at approximately $\theta_1=30^\circ$. These results are attributable to the strong interactions among the rods and the reduction in the rotational symmetry. Figures 4(c) and 4(d) plot the H3 gap width for inner and whole rod rotations, respectively. As shown in the diagrams, the gap width associated with the inner-rod rotation increases with the rotating angle, but that associated with the whole rod rotation approaches to zero at around $\theta_1=\theta_2=40°$. The results associated with the inner rod rotation are governed mainly by the shape of the rod, and those associated with the whole rod rotation are governed by the angle of rotation.

Figure 5 plots the *E*-polarization gap width at $\alpha_1=\alpha_2=1.6$ as a function of rotating angle. The gap widths in E1 (between the seventh and eight bands) and E2 (between the

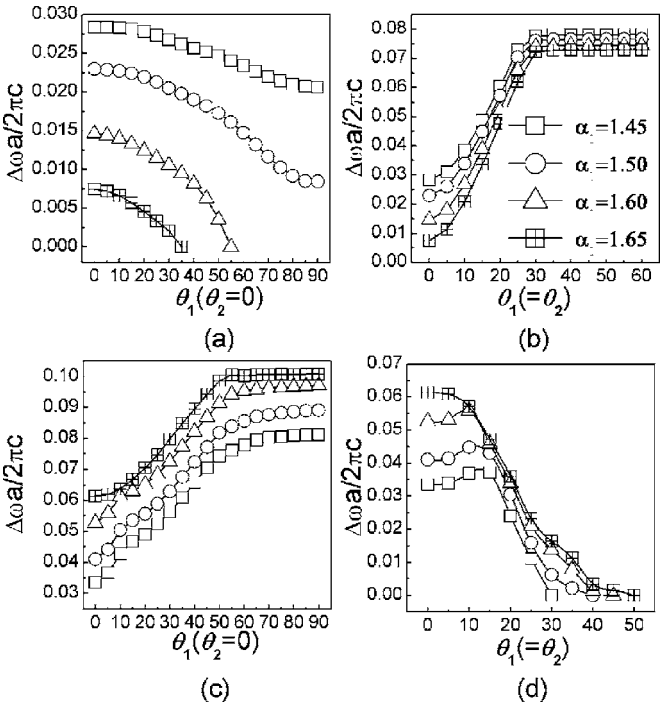

FIG. 4. Gap widths as a function of rotating angles θ_1 and θ_2 for inner rod and whole rod rotations with various $\alpha_1(=\alpha_2)$. H1 gap width for (a) inner rod rotations, $\theta_2=0$, and (b) whole rod rotations, $\theta_2=\theta_1$; H3 gap width for (c) inner rod rotations, $\theta_2=0$, and (d) whole rod rotations, $\theta_2=\theta_1$. Each curve in the same line style in (a), (c), and (d) corresponds to the same quantity of α_1 as the list inserted in (b).

ninth and tenth bands) vary slightly with the rotation of the whole rod, but vary markedly with the rotation of the inner rod. These results may also be understood by considering the field distribution within the hollow oval rods. Figures 6(a) and 6(b) plot the amplitude of the displacement field with inner rod rotation and whole rod rotation through an angle of 30°. The field distribution in the whole rod rotation is identical to that in Fig. 3(b) because the shapes of the hollow oval rods do not change, so the *H*-polarization gap widths are almost the same at all angles of rotation. Moreover, the number of nodal planes associated with inner rod rotation almost

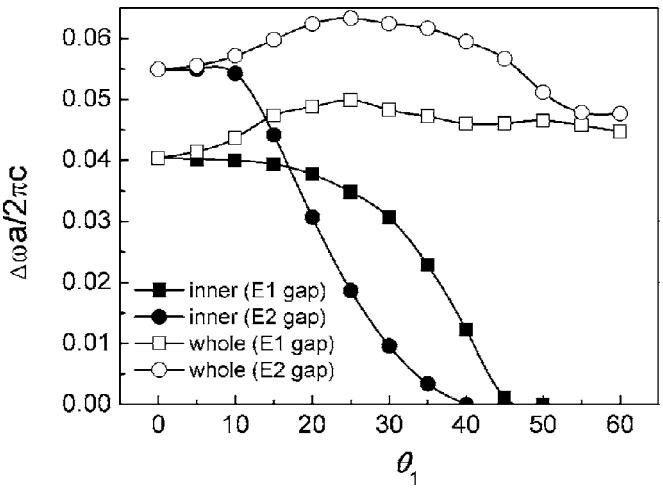

FIG. 5. E1 and E2 gap widths as a function of rotating angle θ_1 for inner rod and whole rod rotations at $\alpha_1=\alpha_2=1.6$.

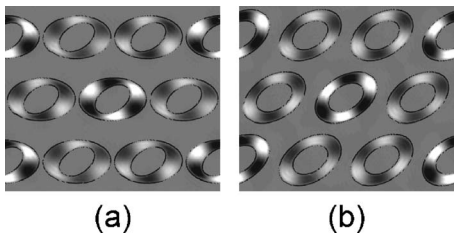

FIG. 6. Displacement-field distribution of *E*-polarization mode inside the hollow oval rods for (a) the inner rod rotation with $\theta_1=30°$ and $\theta_2=0°$ and (b) the whole rod rotation with $\theta_1=\theta_2=30°$ at the *K*-symmetry point and $\alpha_1=\alpha_2=1.6$.

equals that associated with whole rod rotation. However, the fields in the thin dielectric regions are expelled from the dielectric region when the inner rods are rotated, strongly influencing the *E*-polarization band structures. Interestingly, the shapes of individual rods dominate the *E*-polarization band structures,[20] even though the rotational symmetry of the hollow structure is broken.

Figures 7(a) and 7(b) plot absolute PBG as a function of angle associated with inner and whole rod rotation at $\alpha_1=\alpha_2=1.6$. The absolute gap widths of the inner rod rotation vary markedly because they are governed by the *E*-polarization modes. The absolute gap widths under whole rod rotation decline as the angle of rotation increases because they are dominated by the *H*-polarization modes. The properties of the formed absolute PBGs also have the same results for any $\alpha_1(=\alpha_2)$ value.

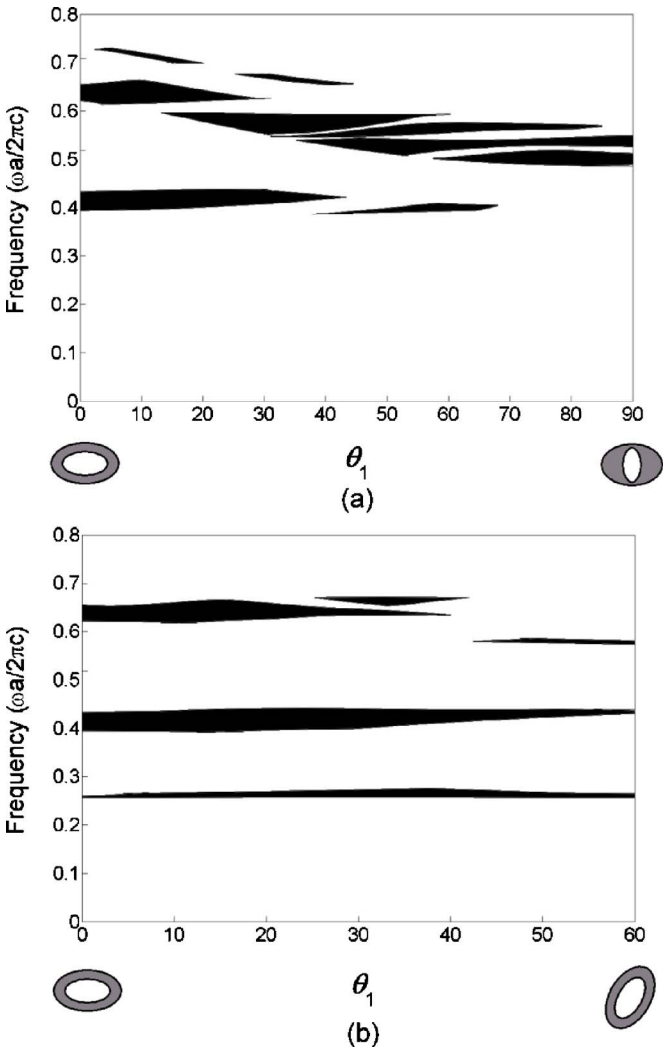

FIG. 7. Absolute photonic band gap as a function of rotating angle θ_1 for (a) inner rod rotations and (b) whole rod rotations at $\alpha_1=\alpha_2=1.6$.

Our simulation and analysis assume that the height of rods is infinity or much larger than the lattice constant of the 2D crystalline arrays. Practically and macroscopically, if the height of the rods is an order larger than the beam size of perpendicular (to the rods) incident light, the height of rods can be considered as infinity ideally. Microscopically, for the case of perpendicular incidence to the rods, if the height of the rods is an order larger than the light wavelength, the wave phenomena of light can be neglected along the direction of rods and the height of rods can be considered infinity. So for the structures we considered here, the minimal height of the rods should be larger than tens of microns to ensure the calculation results agree well with the results for the exact 2D array photonic crystals. For the smaller height of the rods, our analysis and comments would be comparatively applicable or valid until the photonic crystals become critically three-dimensional (3D) confined systems.

IV. CONCLUSION

In this work, the plane-wave method is used to calculate the field patterns and the band structure of a triangular lattice of hollow Te rods. Firstly, three deformed structures are designed by altering the geometric parameters of rods to investigate the effect of structural symmetry on *E*- and *H*-polarization modes. The results in the *H*-polarization modes indicate that the air space among the rods dominates the low-frequency gaps while the shape of the rods affects mainly the high-frequency gaps. The results in the *E*-polarization modes indicate a strong relationship between the shape of the rods and the band gaps, as determined from the field patterns. Two rotations, inner and whole rod rotations, are considered with fixed geometric parameters to investigate the effect of rotational symmetry on *E*- and *H*-polarization modes. The effect on the *E*-polarization mode for rotational structures is similar to that for deformed structures. However, *H*-polarization modes are affected not only by the field distribution among rods but also by the reduction of rotational symmetry. Analyzing the structural and rotational symmetry of the hollow structure is useful in understanding the properties of the formed PBGs and provides a path for designing proper photonic crystal structures with desired PBGs.

ACKNOWLEDGMENTS

The authors would like to thank Professor T. J. Yang and Professor D. S. Chuu for valuable discussion. This work was supported by the National Science Council, Taiwan under Grant No. NSC 94-2112-M-009-001.

[1]E. Yablonovitch, Phys. Rev. Lett. **58**, 2059 (1987).
[2]H. Y. Sang, Z. Y. Li, and B. Y. Gu, Phys. Rev. E **70**, 066611 (2004).
[3]L. D. A. Lundeberg, D. L. Boiko, and E. Kapon, Appl. Phys. Lett. **87**, 241120 (2005).

[4]D. Labilloy *et al.*, Phys. Rev. Lett. **79**, 4147 (1997).
[5]S. G. Lee, S. S. Oh, J. E. Kim, H. Y. Park, and C. S. Kee, Appl. Phys. Lett. **87**, 181106 (2005).
[6]X. H. Wang, B. Y. Gu, Z. Y. Li, and G. Z. Yang, Phys. Rev. B **60**, 11417 (1999).
[7]N. Malkova, S. Kim, and V. Gopalan, Phys. Rev. B **66**, 115113 (2002).
[8]M. Plihal and A. A. Maradudin, Phys. Rev. B **44**, 8565 (1991).
[9]K. Busch and S. John, Phys. Rev. E **58**, 3896 (1998).
[10]R. Wang, X. H. Wang, B. Y. Gu, and G. Z. Yang, J. Appl. Phys. **90**, 4307 (2001).
[11]L. L. Lin and Z. Y. Li, Phys. Rev. B **63**, 033310 (2001).
[12]R. Hillebrand and W. Hergert, Solid State Commun. **115**, 227 (2000).
[13]C. M. Anderson and K. P. Giapis, Phys. Rev. B **56**, 7313 (1997).
[14]N. Susa, J. Appl. Phys. **91**, 3501 (2002).
[15]T. Pan, F. Zhuang, and Z. Y. Li, Solid State Commun. **129**, 501 (2004).
[16]Z. Y. Li, B. Y. Gu, and G. Z. Yang, Phys. Rev. Lett. **81**, 2574 (1998).
[17]E. D. Palik, *Handbook of Optical Constants of Solids* (Academic, New York, 1991).
[18]S. Ades and C. H. Champness, J. Appl. Phys. **49**, 4543 (1978).
[19]J. D. Joannopoulos, R. D. Mead, and J. N. Winn, *Photonic Crystals: Modeling the Flow of Light* (Princeton University Press, Princeton, 1995).
[20]E. Lidorikis, M. M. Sigalas, E. N. Economou, and C. M. Soukoulis, Phys. Rev. Lett. **81**, 1405 (1998).